Fingerprinting local controls on the Neoproterozoic carbon cycle with the isotopic record of Cryogenian carbonates in the Panamint Range, California

Lyle L. Nelson [a,*], Anne-Sofie C. Ahm [b], Francis A. Macdonald [c], John A. Higgins [b], Emily F. Smith [a]

[a] *Department of Earth and Planetary Sciences, Johns Hopkins University, Olin Hall, Baltimore, MD 21218, USA*
[b] *Department of Geosciences, Princeton University, Guyot Hall, Princeton, NJ 08544, USA*
[c] *Department of Earth Science, University of California Santa Barbara, Webb Hall, Santa Barbara, CA 93106, USA*

ARTICLE INFO

ABSTRACT

Neoproterozoic carbon isotope excursions are commonly attributed to changes in the global fraction of organic carbon burial associated with climate instability and/or oxygenation. Here we show that carbonate sediment deposited during the ca. 661 – <651 Ma Cryogenian non-glacial interlude between the Sturtian and Marinoan glaciations exhibit lateral offsets in carbonate-carbon isotope values from coeval units by as much as 10‰. Within the Thorndike submember of the Cryogenian succession in the Panamint Range, California, USA, carbonate-carbon isotope values can be linked to a laterally discontinuous dolomitization front: limestones exhibit $\delta^{13}C_{carb}$ values of ∼+4 to +9‰, whereas values of stratigraphically equivalent dolostones are consistently lower, between ∼-4 and +4‰. Field observations and analyses of clasts from the overlying Marinoan glacial diamictite show that the offset in $\delta^{13}C_{carb}$ values resulted from pre- to syn-Marinoan dolomitization. Further, $\delta^{44/40}Ca$ and $\delta^{26}Mg$ data indicate that this isotopic variability resulted from sediment-buffered diagenesis. We propose that extremely positive $\delta^{13}C_{carb}$ values record local primary productivity within restricted platform surface waters and/or oxygenated pore fluids and negative values reflect anaerobic remineralization of organic carbon within sediment pore waters. In this scenario, neither the original calcite/aragonite nor subsequent dolomite precipitates of the Thorndike submember record $\delta^{13}C_{carb}$ values that are representative of global Cryogenian seawater, and instead they archive the evolution of local dissolved inorganic carbon pools.

© 2021 Elsevier B.V. All rights reserved.

1. Introduction

Carbon isotope ($\delta^{13}C$) data from shallow marine carbonate strata have long been used to reconstruct temporal shifts in the isotopic composition of seawater, correlate between stratigraphic sections regionally and globally, and construct chemostratigraphic age models (e.g., Saltzman and Thomas, 2012). The underlying assumption is that the $\delta^{13}C$ values of carbonate rocks reflect the composition of dissolved inorganic carbon (DIC) in seawater and are buffered from the effects of post-depositional diagenetic alteration (Banner and Hanson, 1990). This concept is substantiated by globally reproducible results in the Phanerozoic Eon, supported by both radiometric ages and biostratigraphy, and thus has been applied to the $\delta^{13}C$ record of the Proterozoic and Archean eons

(e.g., Shields and Veizer, 2002; Halverson et al., 2005). Under this interpretation, and assuming the sampled carbonates are representative of the contemporaneous average global carbonate sink (Blättler and Higgins, 2017), $\delta^{13}C$ excursions through Earth history chronicle secular changes in the net global fluxes of organic carbon burial and oxidation, and can be linked to changes in the climate, environment, and biosphere.

Carbonate strata from the Neoproterozoic Era preserve highly variable $\delta^{13}C$ records, particularly those deposited before, in-between, and after the Cryogenian snowball Earth glaciations (Hoffman and Schrag, 2002; Halverson et al., 2005). Carbonates for most of the Cryogenian non-glacial interlude – the >10 m.y. ice-free interval in between the end of the Sturtian glaciation and before the onset of the Marinoan glaciation (Rooney et al., 2020; Nelson et al., 2020) – record ^{13}C-enriched $\delta^{13}C$ values (∼+5 to +10‰) sometimes referred to as the Keele peak (e.g., Halverson et al., 2005). This and other protracted Neoproterozoic stratigraphic intervals recording positive $\delta^{13}C$ values have been interpreted as record-

ing a high proportion of organic carbon burial, corresponding to high rates of oxidant accumulation within surface environments (e.g., Knoll et al., 1986). The Cryogenian non-glacial interlude is punctuated by what are thought to be three distinct large negative δ^{13}C excursions: the Rasthof (Hoffman and Schrag, 2002), Taishir (Johnston et al., 2012; Bold et al., 2016), and Trezona anomalies (Swanson-Hysell et al., 2010). When interpreted globally, these negative excursions both before and after the Cryogenian snowball Earth glaciations have been linked to a shutdown in biological productivity (Hoffman and Schrag, 2002), destabilization of methane hydrates following warming (Kennedy et al., 2001), oxidation of a methane greenhouse (Schrag et al., 2002), changes in anaerobic respiration due to an increase in organic carbon export (Tziperman et al., 2011), and the combined effect of a rapidly increasing global temperature and CO_2 drawdown (Higgins and Schrag, 2003).

Others have viewed the extreme fluctuations observed in the Neoproterozoic δ^{13}C record as difficult to interpret in a mass-balance framework due to the dramatic changes in oxidants that are implied, and have suggested alternative possibilities including: the existence of an unusually large pool of authigenic carbonate as a significant component of the global carbon cycle (Schrag et al., 2013), the existence of an unusually large reservoir of marine organic carbon to allow non-steady-state behavior (Rothman et al., 2003), and diagenetic origins for large excursions, related to either burial or meteoric fluids (Knauth and Kennedy, 2009; Derry, 2010). Additionally, studies on modern carbonate platforms have demonstrated that early marine diagenesis and aragonite production in platform top environments can result in variable δ^{13}C chemostratigraphic curves that are not accurate records of open-marine DIC fluctuations (Swart, 2008; Oehlert and Swart, 2014), but rather records of the relative contributions of sediment-buffered versus fluid-buffered diagenetic precipitates (Ahm et al., 2018; Higgins et al., 2018). Using this framework, Ahm et al. (2019) invoked a diagenetic origin for δ^{13}C variability observed in Marinoan cap dolostones globally, known as the Maieberg anomaly. Along similar lines, by examining Neoproterozoic δ^{13}C records from the Otavi Platform in Namibia, Hoffman and Lamothe (2019) concluded that upper foreslope carbonates – strata that are most susceptible to seawater-buffered diagenesis – do not have the excursions of co-eval platform and lower foreslope carbonates, and instead record DIC values akin to the modern ocean. Therefore, they speculate that nucleation kinetics were responsible for the large DIC variability observed on Proterozoic platforms. Bold et al. (2020) showed that early dolomitization fronts blunt the δ^{13}C variability preserved in Cryogenian carbonate successions in Mongolia, corroborating the potential for diagenetic fluids to affect the isotopic composition of carbonate minerals. Close covariation between organic carbon and carbonate δ^{13}C values has been documented for the Rasthof, Keele, Taishir, and Trezona carbon isotope anomalies during the Cryogenian non-glacial interlude, which may suggest primary perturbation to the surface carbon cycle (Swanson-Hysell et al., 2010; Johnston et al., 2012), although covariation between organic and carbonate δ^{13}C can be produced locally in platform and periplatform environments (Oehlert and Swart, 2014). Clearly, the origin, geographic variability, synchroneity, and significance of these large Cryogenian carbon isotope excursions remain uncertain.

Here, we present new δ^{13}C, calcium isotope ($\delta^{44/40}$Ca) and magnesium isotope (δ^{26}Mg) data from Cryogenian non-glacial interlude carbonate strata in the Panamint Range of Death Valley, California (Fig. 1). We observe significant δ^{13}C variability associated with a mapped dolomitization front and different sedimentary environments, and assess the origins of these trends using geochemical tracers of diagenesis ($\delta^{44/40}$Ca and δ^{26}Mg) and interpretation of the evolving depositional setting. Our results suggest that observed variability can be explained by evolution of local DIC

pools rather than global seawater, which may inform interpretations of Neoproterozoic carbonate platform geochemical records.

2. Geological setting

The Panamint Range of southeastern California hosts a <2 km-thick Cryogenian succession, the Kingston Peak Formation (Fig. 1; Miller, 1985; Prave, 1999), which was deposited during multiple episodes of rifting on the southwestern margin of Laurentia related to the protracted breakup of Rodinia (Prave, 1999; Nelson et al., 2020) and outcrops for >60 km along both limbs of a doubly plunging anticline (Fig. 1D). The Kingston Peak Formation includes two distinct intervals of massive diamictite interpreted as glacial in origin, the Surprise Member and Wildrose submember (Miller, 1985), which have been correlated to the Sturtian (∼717–661 Ma) and Marinoan (<651–635 Ma) snowball Earth glaciations based on the lithostratigraphy and δ^{13}C compositions of overlying cap carbonates, the Sourdough Limestone Member and Noonday Formation, respectively (Fig. 1B; Prave, 1999; Petterson et al., 2011). More recently, these correlations were confirmed with high-precision geochronological constraints (Fig. 1; Nelson et al., 2020).

The Sourdough Limestone Member and Middle Park, Mountain Girl, and Thorndike submembers of the South Park Member compose a <1 km succession of mixed siliciclastic and carbonate strata deposited during the Cryogenian non-glacial interlude. The Sourdough Limestone Member is a finely laminated dark blue limestone that sharply overlies the Surprise Member diamictite, and is up to 35 m thick (Fig. 2A). In most sections, this is gradationally overlain by the Middle Park submember of the South Park Member, which reaches 180 m in thickness and comprises siltstone to shale with minor thin beds of finely laminated silty limestone (Fig. 2B) and arkosic turbidites. In some sections, arkosic grit channels in the basal Middle Park submember erosively remove much or all of the Sourdough Limestone Member. These post-Sturtian units are unconformably overlain by erosive conglomerate of the Mountain Girl submember, which grades into crossbedded quartz sandstone. Shoreface sandstone of the Mountain Girl submember grades into sandy carbonate and carbonate of the Thorndike submember, which is up to 100 m thick. Carbonate rocks of the Thorndike submember are largely recrystallized, but frequently preserve ripple cross-laminated and cross-bedded textures delineated by quartz grains (Fig. 2C,D), indicating they are primarily grainstone. Locally, microbialite structures occur (Fig. 2E,F). Near the top of the Thorndike submember, there are intraformational exposure surfaces, demarcated by thin layers of pebble conglomerate to sandstone underlain by sandstone- or breccia- filled karst pipes (Fig. 2G-J). A clastic bed ∼15 m below the top contact of the Thorndike has a maximum depositional age of 651.7±0.6 Ma (Nelson et al., 2020). The Thorndike submember is unconformably overlain by diamictite of the Wildrose submember, which in some locations cuts as low as Mesoproterozoic basement (Miller, 1985; Prave, 1999).

Although other Neoproterozoic strata are exposed throughout the Death Valley region, units deposited during the Cryogenian non-glacial interlude are only exposed in the Panamint Range (along ∼80 km of strike). Within Cryogenian strata, there are four angular unconformities, and evidence for active syn-sedimentary faulting, basement uplift, and structural generation of topographic highs at multiple stratigraphic levels (Miller, 1985; Prave, 1999). Sedimentary evidence for basin restriction during the Cryogenian includes abrupt lateral facies and thickness variations within units, karst horizons, fine laminations that resemble seasonal varves, coarse debris flows, alluvial and fluvial depositional systems, and uranium-, sulfide-, and graphite-enrichments (Fig. 2; Carlisle et al., 1980; Miller, 1985). Taken together, these observations sug-
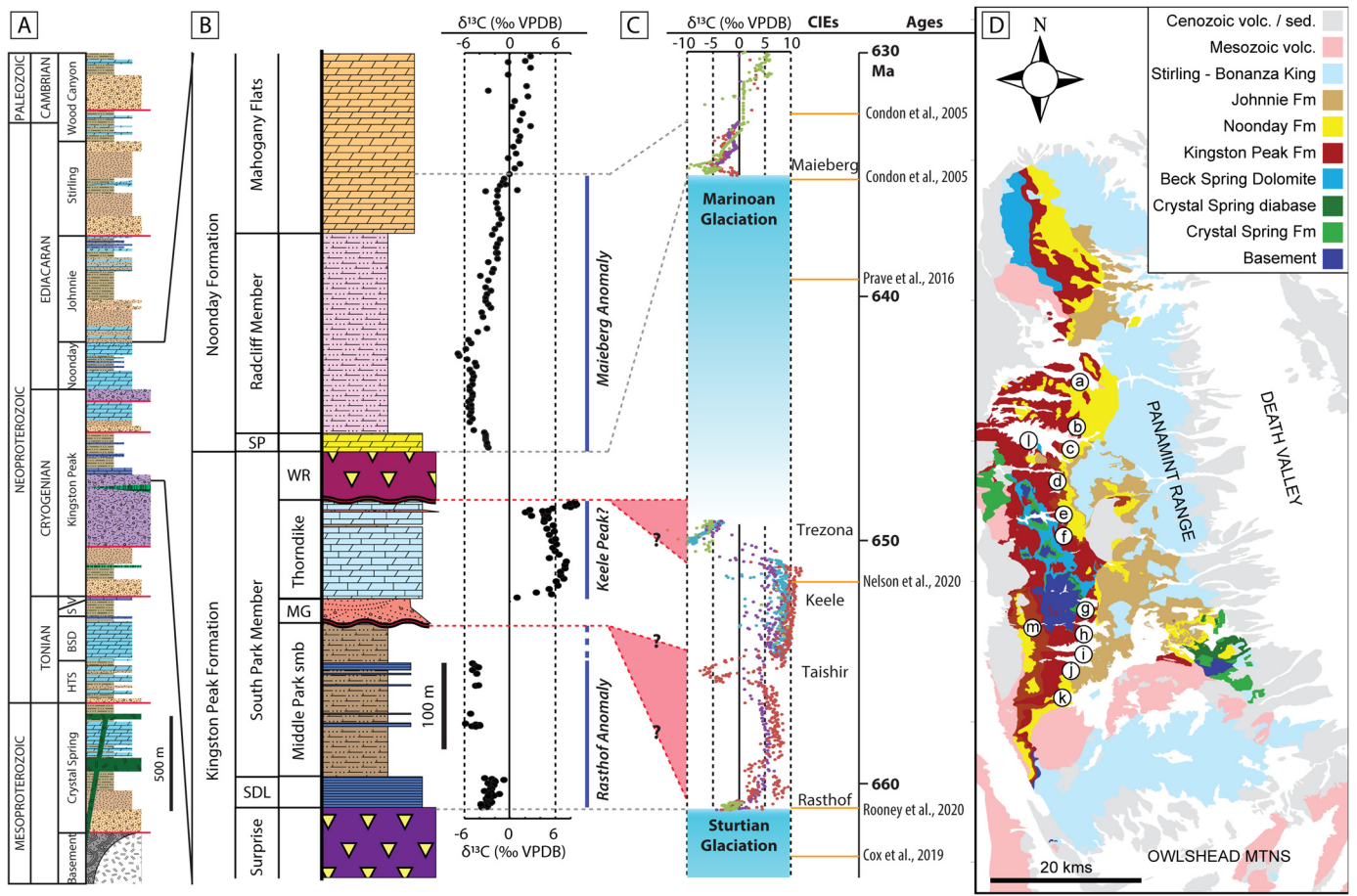
Fig. 1. A) Generalized stratigraphy of Death Valley. B) Composite chemostratigraphy of the Panamint Range. Sourdough data from South Park (L1509), Middle Park data from Pleasant Canyon (L1503), lower Thorndike data from Surprise Canyon (L1630), upper Thorndike data from Redlands Canyon (L1603), Sentinel Peak and Radcliff data from Wildrose Canyon (L1803), Mahogany Flats data from Wildrose Canyon (Petterson et al., 2011). C) Composite carbon isotope profile of the Cryogenian. Green data points from NW Canada (Johnston et al., 2012); purple data points from Namibia (Halverson et al., 2005); Blue data points from Australia (Swanson-Hysell et al., 2010); red data points from Mongolia (Bold et al., 2016). Red lines are unconformities. D) Generalized map of Panamint Range with specific localities labeled to correspond to sections in Figs. 3 and 4. Abbreviations: HTS—Horse Thief Springs Formation; BSD—Beck Spring Dolomite; S—Saratoga sandstone; V—Virgin Spring Limestone; SDL—Sourdough Limestone Member; SP—Sentinel Peak Member; MG—Mountain Girl submember; WR—Wildrose submember; VPDB—Vienna Peedee Belemnite; CIEs—Carbon Isotope Excursions. (For interpretation of the colors in the figure(s), the reader is referred to the web version of this article.)

gest sediment deposition was in locally formed basins generated by tectonic subsidence associated with the incipient rifting of this margin (Miller, 1985), which may have been partially-restricted from open marine environments.

Previous chemostratigraphic studies in the Death Valley region have documented negative $\delta^{13}C$ values in the Sourdough and Noonday, which have been correlated to the Rasthof and Maieberg negative $\delta^{13}C$ anomalies, respectively (Prave, 1999; Corsetti and Kaufman, 2003; Petterson et al., 2011). Additionally, there are some previously published $\delta^{13}C$ values from the Thorndike submember in the Panamint Range: Prave (1999) published three data points from Redlands Canyon with values of $\sim+6‰$; Corsetti and Kaufman (2003) published values of $\sim+5‰$ from Tucki Mountain; and Petterson et al. (2011) published scattered values ranging from ~-4 to $+8‰$ from sections in Wood Canyon and near the town-site of Skidoo in their Data Repository.

Metamorphic grade varies significantly across the Panamint Range. Rocks exposed along the western limb of the anticline and in the northern part of the range were subject to Mesozoic sillimanite-grade metamorphism and local marbleization (Labotka et al., 1985). However, rocks on the eastern limb – particularly in the central and southern Panamint Range – are greenschist-grade or lower. While this metamorphism and localized strain can locally change unit thicknesses, it has not significantly altered $\delta^{13}C$ within

carbonate units as demonstrated by lateral $\delta^{13}C$ consistency in the Noonday Formation (Petterson et al., 2011).

3. Methods

Mapping of Cryogenian strata throughout the Panamint Range was conducted between 2015-2018 at 1:10,000 scale. Twenty-six stratigraphic sections were measured in a north-south transect along ~50 km of strike, focusing on the lower-grade rocks within the eastern limb of the Panamint anticline. Within carbonate-bearing units, fist-sized carbonate samples were collected at 0.5 to 3-m resolution.

Fresh cut surfaces were microdrilled for powder along laminations, avoiding veins and siliciclastic grains. Samples were analyzed for carbonate carbon and oxygen isotopic compositions ($\delta^{13}C$ and $\delta^{18}O$) on a VG Optima dual inlet mass spectrometer at the Harvard University Laboratory for Geochemical Oceanography. Approximately 1 mg of powder was reacted in a common orthophosphoric acid bath at 90 °C with a magnetic stirrer. Evolved CO_2 was collected cryogenically and analyzed using an in-house reference gas. Memory effects are estimated at <0.1‰ based on variability of standards. Isotopic results are reported in per mil (‰) notation relative V-PDB (Vienna-Pee Dee Belemnite) by using an in-house Cararra Marble standard that was calibrated against several NBS carbonate standards and cross-calibrated with other laboratories.
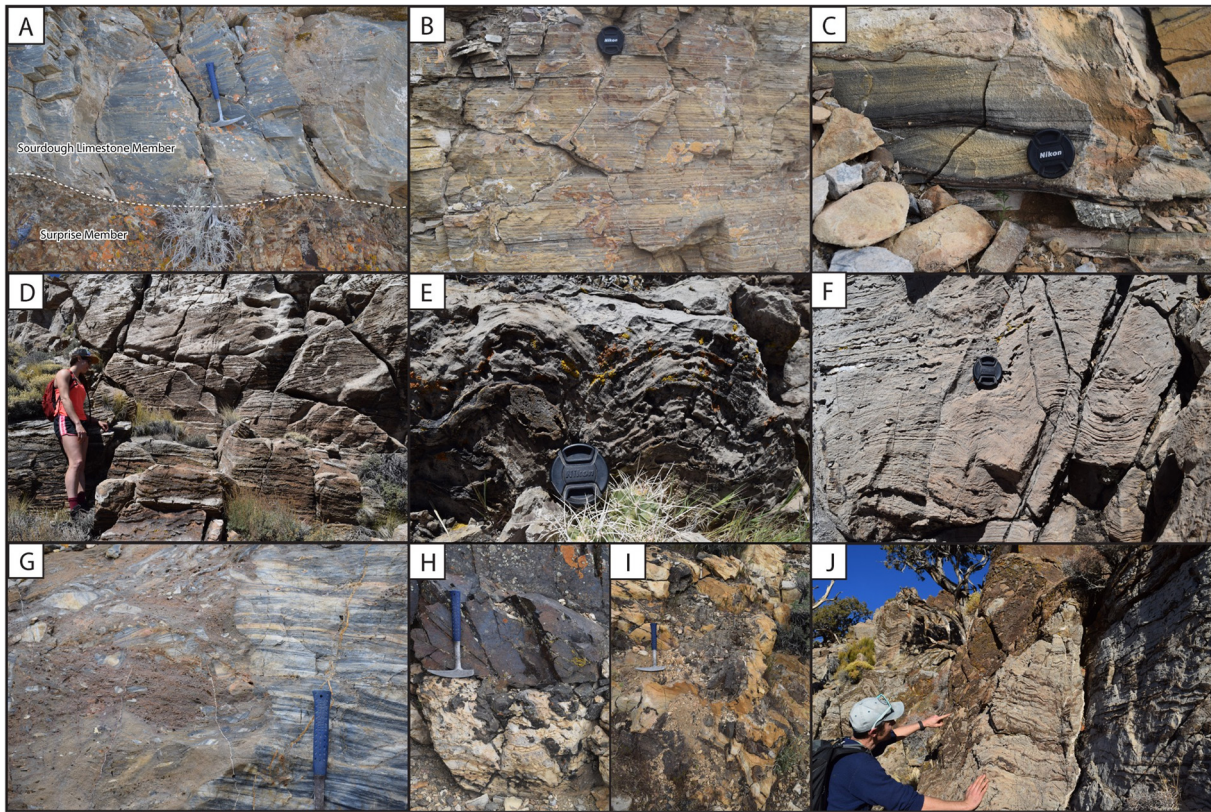
Fig. 2. Field photographs of Sourdough Limestone Member, Middle Park submember, and Thorndike submember. Lens cap is 5.2 cm in diameter. Hammer is 33 cm long. A) Finely laminated dark blue limestone in basal Sourdough Limestone Member (Sturtian cap carbonate) sharply overlying Sturtian diamictite of the Surprise Member. B) Finely laminated limestone and siltstone of Middle Park submember. C) Ripple cross lamination in carbonate grainstone of the Thorndike submember. D) Large foresets in cross-bedded sandy carbonate grainstone of the Thorndike submember. E, F) Microbial carbonate with stromatolites within the Thorndike submember. G, H, I, J) Karst-related grikes infilled with sand and/or carbonate breccia within the upper Thorndike submember.

Standard deviation (1σ) from standards was better than $\pm0.1\%$ for $\delta^{13}C$ and $\delta^{18}O$.

Diamictite carbonate clast samples from the Wildrose submember, sampled between Redlands Canyon and South Park, were analyzed at the Johns Hopkins University Isotope Ratio Mass Spectrometer Laboratory. Samples were analyzed for $\delta^{13}C$ and $\delta^{18}O$ isotopic compositions using a GasBench II peripheral device coupled to a Thermo-Finnigan MAT253 isotope ratio mass spectrometer (IRMS) in continuous-flow mode. Approximately 0.3 mg of sample powder reacted with 100% phosphoric acid in helium-purged vials at 30 °C, overnight. Evolved CO_2 gas was then analyzed against tank CO_2 gas and isotopic results normalized to V-PDB ‰ scale using working in-house carbonate standards (ICM, Carrara Marble and IVA Analysentechnik, calcium carbonate) that are calibrated against international standards NBS-18 and IAEA-603. Standard deviation (1σ) of $\delta^{13}C$ and $\delta^{18}O$ values for in-house standards was <0.02‰ and <0.14‰, respectively.

The following sections were selected for analyses of trace element compositions and $\delta^{44/40}Ca$ and $\delta^{26}Mg$ isotopes: 1) one section of the Sourdough Limestone Member and Middle Park submember (L1509), 2) three sections of the Thorndike submember, including one limestone section (L1509), one dolostone section (L1502), and one section of mixed carbonate mineralogy (L1603). At Princeton University, 5 mg of carbonate powder from each sample were dissolved in 5 mL 0.1N buffered acetic acid and allowed to react for 4 hours in order to dissolve the carbonate without leaching the less soluble siliciclastic components. Following dissolution, the supernatant was centrifuged and separated from the insoluble residue.

To purify Ca and Mg, samples were processed through an automated high-pressure ion chromatography system (Dionex UCS-5000+) following previously established methods (e.g., Higgins et al., 2018). The purified samples were analyzed for $\delta^{44/40}Ca$ and $\delta^{26}Mg$ values on a Thermo Scientific Neptune Plus Multicollector-Inductively Coupled Plasma-Mass Spectrometer (MC-ICP-MS) at Princeton University, using standard sample-standard bracketing techniques to correct for instrumental mass bias. Calcium isotope measurements were carried out at medium resolution to avoid ArHH$^+$ interferences. All samples were diluted to match standard concentrations within 10% in order to ensure comparable levels of ArHH$^+$ based interference across samples and bracketing standards, and in order to minimize concentration-dependent isotope effects. Samples were measured twice within the same run, and some sample were re-measured over multiple runs.

All data are reported in delta notation relative to a known standard, and the reported delta value is the average of the repeated measurements. The 2σ uncertainty for each sample can be found in the supplementary data table. For Ca isotopes, the measured $\delta^{44/42}Ca$ values are converted to $\delta^{44/40}Ca$ values relative to modern seawater assuming mass dependent fractionation with a slope of 2.05. For Mg isotopes, measured $\delta^{26}Mg$ values are reported relative to DSM-3. Long-term external reproducibility for each isotope system is determined based on the standard deviation of known standards taken through the full chemical procedure with each batch of samples. For Ca isotopes, the external reproducibility for SRM915b and SRM915a relative to modern seawater is -1.17±0.15‰ (2σ, N=41) and -1.86±0.16‰ (2σ, N=24), respectively. For Mg isotopes, the long-term reproducibility for Cambridge-1 and seawater (PSW) are -2.57±0.11‰ (2σ, N=11) and -0.81±0.13‰ (2σ, N=22), respectively.

The Sr/Ca, Mn/Ca, and Mg/Ca ratios were measured on aliquots of dissolved powders analyzed for $\delta^{44/40}Ca$ and $\delta^{26}Mg$. Measure-
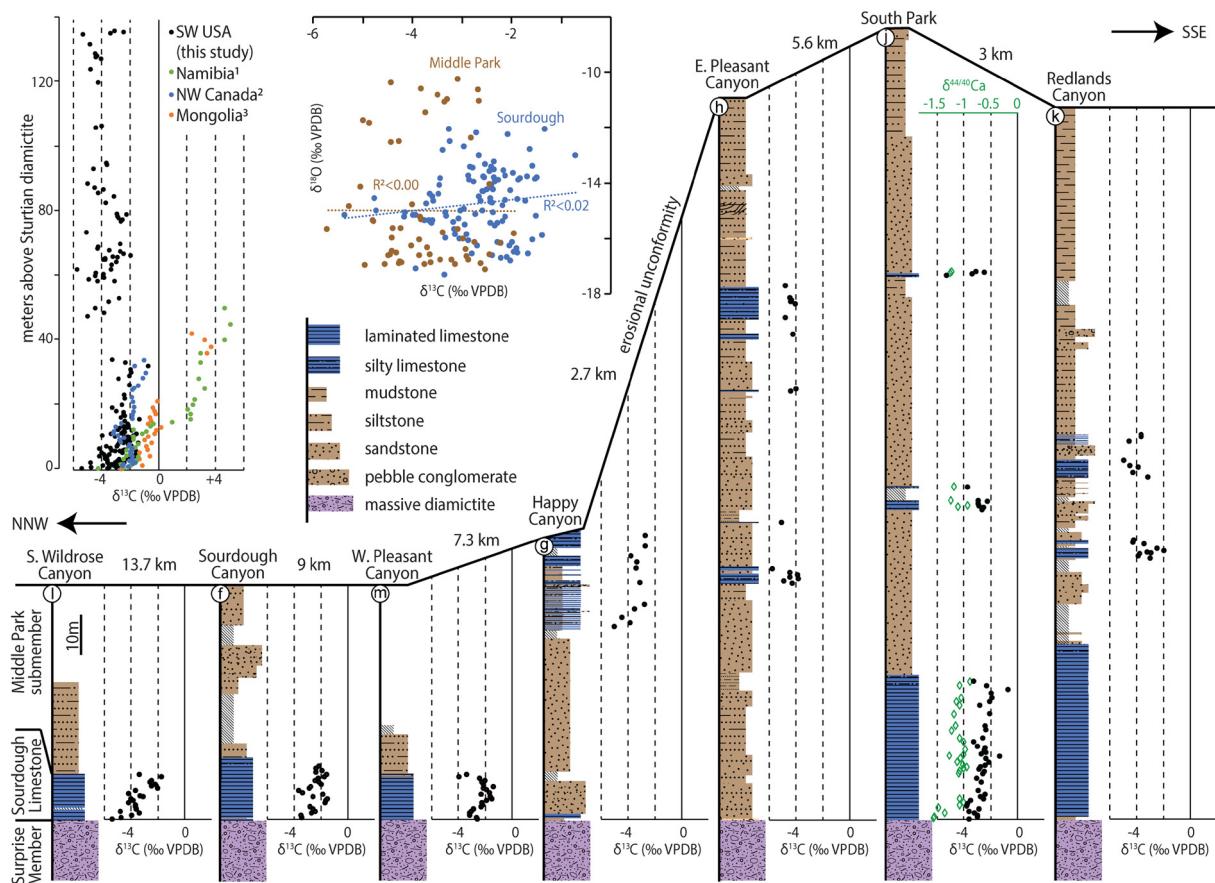
Fig. 3. Lithostratigraphy and chemostratigraphy of the Sourdough Limestone Member and Middle Park submember. Sections correspond to labels in Fig. 1. Post-Sturtian δ^{13}C data from the Panamint Range are compared to corresponding data from Namibia (Halverson et al., 2005), NW Canada (Johnston et al., 2012), and Mongolia (Bold et al., 2016).

ments were performed using a Thermo Finnegan iCAP Q Inductively Coupled Plasma Mass Spectrometer (ICP-MS). The metal to Ca ratios were determined using a set of matrix-matched in-house standards spanning the sample concentration. The external reproducibility of the metal to calcium concentrations is estimated at >90% (N=29) from replicate measurements of the SRM-88b standard. All geochemical data tables from this study are available in the supplementary material.

4. Results

Carbon isotope values from the Sourdough Limestone Member and overlying Middle Park submember are all negative, ranging from -5.7 to -0.7‰ (Fig. 3). The majority of δ^{13}C values for the Sourdough Limestone Member are between -4 and -2‰, with a generally positive, but scattered, trend up-section. Data from the Middle Park submember are more scattered, but most values are between -5 and -2‰. There is no generalized trend, and significant scatter (>2‰) is also observed over short length scales and within individual beds (Fig. 3). Within these units, δ^{13}C and δ^{18}O values do not strongly covary (r^2<0.02; Fig. 3). The basal 3 m of the Sourdough Limestone have $\delta^{44/40}$Ca values between -1.6 and -1.3‰, expected values for neomorphosed aragonite precipitates (Ahm et al., 2018; Higgins et al., 2018), while samples from the rest of the Sourdough Limestone and from the Middle Park submember range from -1.3 to -0.9‰, within the range of altered aragonite or of modern calcite precipitates from seawater (Gussone et al., 2005, 2020; Figs. 3, 8B,D). Ratios of Sr/Ca range from ~0 to ~4.3 mmol/mol with an average of 1.9 mmol/mol, and Mn/Ca ra-

tios range from ~0 to ~4.1 mmol/mol with an average of 0.75 mmol/mol (Fig. 8D-F).

While carbonate rocks of the Sourdough Limestone Member and the Middle Park submember are exclusively limestone, those of the Thorndike submember vary in mineralogy along strike, with some sections preserved entirely as calcite, some as dolomite, and some with selective dolomitization interfingering with limestone (Figs. 4, 5). Dolomitization boundaries are generally sharp, although within ~1 m of the adjacent limestone diffuse mm-scale veinlets of dolomite are common (Fig. 5C,D). The dolomitization boundaries generally follow bedding horizons, but are irregular and lobate on the outcrop scale (Fig. 5A-C). Dolomitization fronts wedge in and out over relatively short lateral distances and occur within multiple stratigraphic horizons (Figs. 4, 5).

The Thorndike submember has large δ^{13}C variability that tracks mineralogy (Figs. 4–6). In limestone sections, δ^{13}C values range from ~+4 to +7‰, locally rising to +9‰ in the uppermost strata below the Wildrose diamictite. Limestone samples within 1-m of dolostone or siliciclastic beds are generally more negative (-2 to +4‰; Figs. 4–6). Dolomitized Thorndike beds have more δ^{13}C variability, ranging from -4 to +4‰. The correlation between δ^{13}C and mineralogy holds quantitatively with Mg/Ca data from select sections and qualitatively with 10% HCl field tests (Fig. 6A-B). Additionally, δ^{13}C values are more negative in thicker dolomitized intervals than in thinner ones (Fig. 6C). Measured δ^{13}C and δ^{18}O values in Thorndike samples do not covary (r^2=0.13/0.12), and δ^{18}O values range from -19.8 to -6.7‰, with a larger range and a lower average value among limestone samples (Fig. 6B).

Between Redlands and South Park Canyon, clasts of the Wildrose diamictite are almost entirely carbonate and lithologically in-
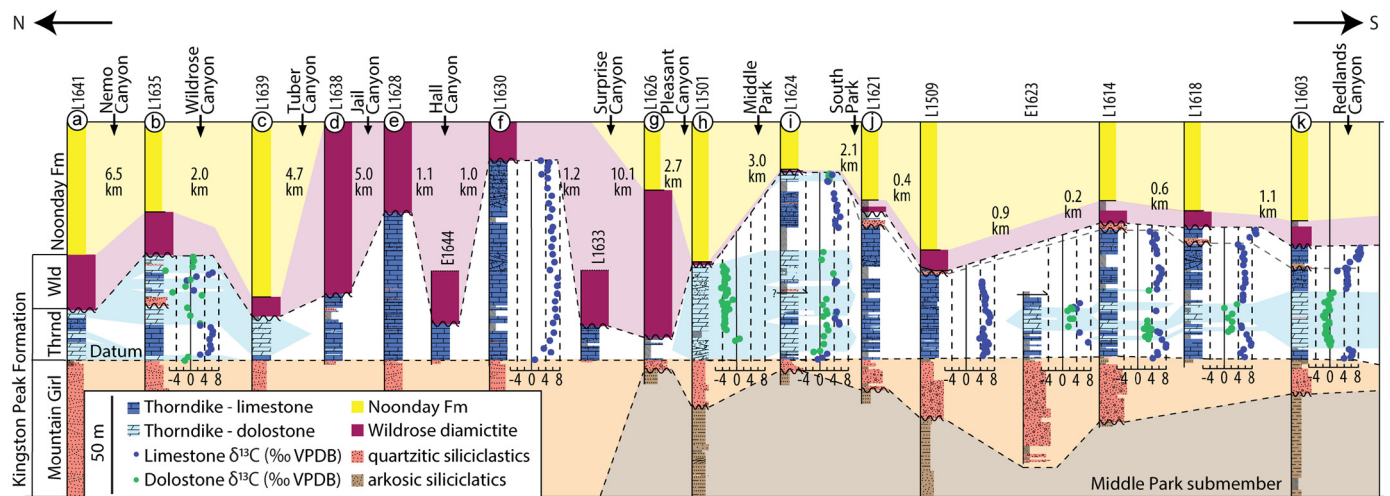
Fig. 4. Lithostratigraphy and $\delta^{13}C$ chemostratigraphy of the Thorndike submember. Sections correspond to labels in Fig. 1. Light blue shade represents dolomitization front.

distinguishable from the underlying Thorndike submember (Fig. 7). Carbonate clasts include laminated light blue limestone, recrystallized white limestone, and orange to tan dolostone (Fig. 7A-E). Limestone clasts have $\delta^{13}C$ values that range from -0.5 to +8.5‰, but most clasts are +4 to +8‰ (Fig. 7F,G). Dolostone clasts range from +0.3 to +3.2‰ and have lower values than most limestone samples (Fig. 7F,G). The majority of these values fall within the same ranges as the values of the underlying *in situ* limestone and dolostone beds of the Thorndike (Fig. 6C). Some dolostone clasts in the Wildrose diamictite are rimmed by calcite, and, in these samples, the rims generally have higher $\delta^{13}C$ values by up to 4‰ and lower and more consistent $\delta^{18}O$ values of ∼-13‰ (Fig. 7D,F).

Within the three analyzed sections of the Thorndike submember, $\delta^{44/40}Ca$ values for both dolostone and limestone samples are between -1.3 and -0.8‰ (Fig. 8), within the range of modern calcite precipitates from seawater (Gussone et al., 2005, 2020). There are no clear relationships between mineralogy and $\delta^{44/40}Ca$ values, or between $\delta^{13}C$ and $\delta^{44/40}Ca$ values (Fig. 8A,B). The $\delta^{26}Mg$ values of dolostone from these sections are between -1.8 and -1.2‰ (Fig. 8), which is ∼1‰ higher than modern seawater-buffered dolomite (values ∼-2.8‰, Higgins and Schrag, 2010). Dolostone $\delta^{44/40}Ca$ and $\delta^{26}Mg$ values do not show a clear relationship (Fig. 8C). Limestone Sr/Ca ratios are scattered and range from ∼0 to ∼1.6 mmol/mol with an average of 0.4 mmol/mol. Dolostone Sr/Ca ratios range from ∼0.1 to ∼0.5 mmol/mol with an average of 0.3 mmol/mol and one outlier of 0.9 mmol/mol (Fig. 8D,E). Limestone Mn/Ca ratios range from ∼0 to ∼2.0 mmol/mol, with an average of 0.5 mmol/mol, and dolostone Mn/Ca ratios range from ∼1.6 to ∼9.4 mmol/mol with an average of 2.9 mmol/mol (Fig. 8F).

5. Discussion

5.1. Chemostratigraphy of the Sourdough and Middle Park

The Sourdough Limestone Member caps glaciogenic diamictite of the underlying Surprise Member and, together with the conformably overlying Middle Park submember, was deposited below wave base during post-Sturtian transgression (Nelson et al., 2020). We document lateral persistence of negative $\delta^{13}C$ values within the Sourdough Limestone Member and thin limestone beds of the Middle Park submember throughout the Panamint Range. Globally, in documented Sturtian cap carbonates, recovery of the Rasthof negative $\delta^{13}C$ excursion to positive values occurs over a short stratigraphic interval—typically within 10 m, and, even in the most expanded sections, within 20-40 m (Fig. 3; Bold et al., 2016;

Hoffman and Schrag, 2002; Halverson et al., 2005)—and presumably relatively rapidly (i.e. <100 kyrs, assuming sedimentation rate >0.1 mm/yr, Hoffman, 2011). Therefore, if the $\delta^{13}C$ values of the Sourdough Limestone Member and Middle Park submember record trends in the composition of global seawater DIC, the persistence of negative values for >130 m (Fig. 3) without a recovery to positive values would suggest rapid sedimentation rates within this basin, preserving an expanded stratigraphic record of the aftermath of the Sturtian glaciation. Such an interpretation is supported by sedimentological evidence consistent with fast sedimentation within the Middle Park submember, including channelized arkosic turbidites and soft-sediment deformation. Yet, the preservation of stratigraphically persistent negative $\delta^{13}C$ values within these units could have also resulted from local depositional conditions unrelated to trends in global seawater through processes which we discuss below.

The negative $\delta^{13}C$ values of the Sourdough Limestone and Middle Park are accompanied by low $\delta^{44/40}Ca$ values (as low as -1.6‰ with an average of -1.13‰; Fig. 3) and relatively high Sr/Ca values (average of 1.9 mmol/mol; Fig. 8), which are consistent with primary platform aragonite sediment for post-Sturtian cap carbonates—analogous to interpretations of aragonite precipitation accompanied by low $\delta^{13}C$ values for post-Marinoan cap carbonates (Ahm et al., 2019). In the Neoproterozoic, low $\delta^{13}C$ values of platform top aragonite have been linked to periods of sea-level rise, during which nutrient-rich and/or DIC-poor platform fluids were pushed to the surface (Ahm et al., 2019). Platform surface waters depleted in ^{13}C could have been generated by kinetic isotope effects due to CO_2 invasion driven by high primary productivity (Lazar and Erez, 1992) or upwelling of platform interior fluids that are out of equilibrium with the atmosphere (Clark et al., 1992). Allochems generated from such platformal carbonates and subsequently transported into more basinal environments could be preserved by sediment-buffered diagenesis (due to fast burial rates and/or minimal subsurface fluid flow in deeper water environments) and therefore record negative $\delta^{13}C$ compositions, low $\delta^{44/40}Ca$ values, and high Sr/Ca values, comparable to those observed in the Sourdough Limestone Member and Middle Park submember.

In a variation from this model, the negative $\delta^{13}C$ values within limestone beds of the Middle Park could be the result of high local primary productivity and subsequent organic carbon remineralization and authigenic carbonate precipitation within pore space. This interpretation is consistent with $\delta^{13}C$ variability of >2‰ within relatively thin stratigraphic intervals (<5 m) or even single beds (Figs. 3, 9A). However, it is difficult to determine the original or-
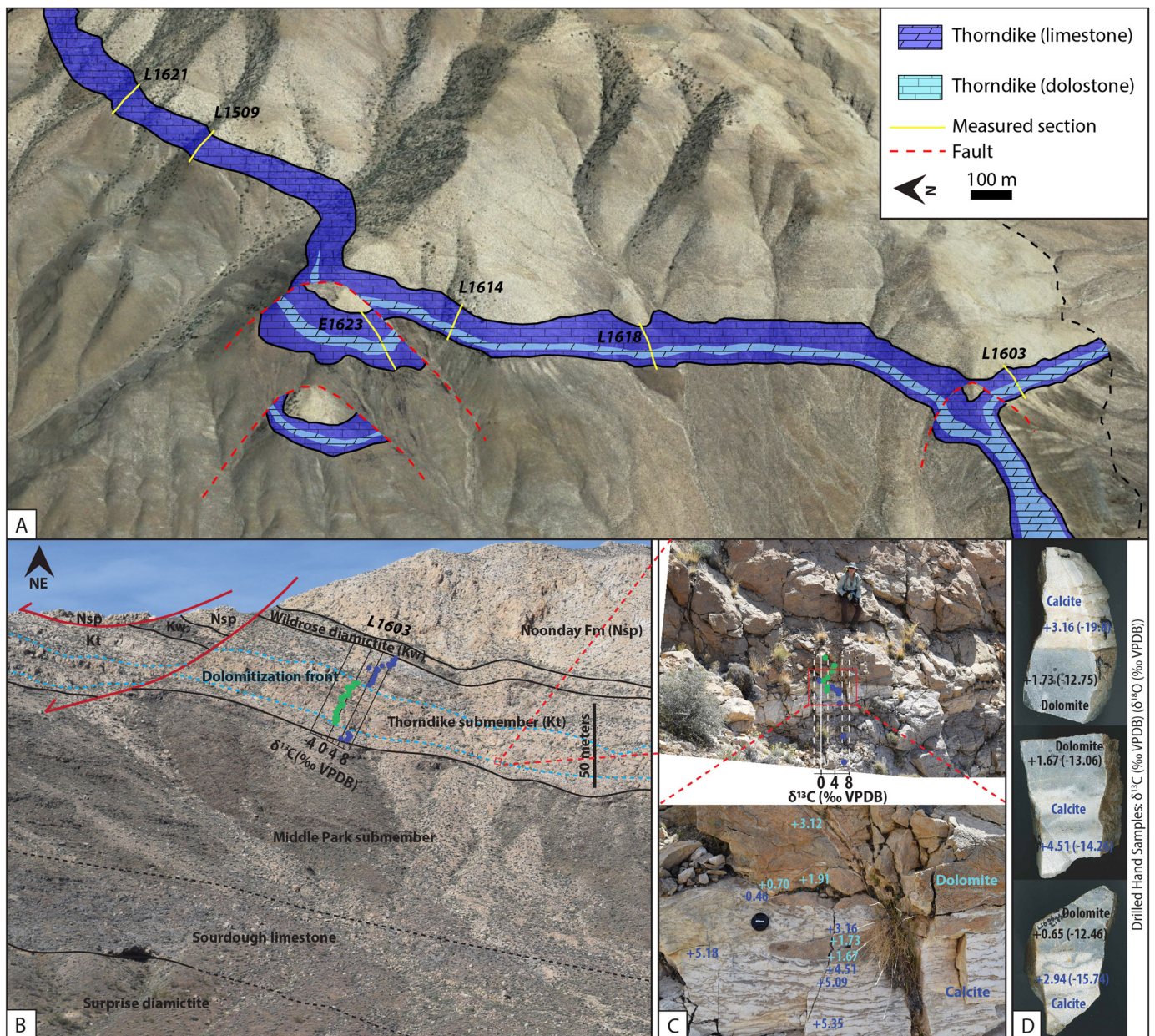
Fig. 5. Alteration of carbon isotopes by dolomitization within the Thorndike submember in Redlands Canyon (section L1603). A) Annotated Google Earth image, demonstrating the spatial extent of laterally variable dolomitization within the Thorndike submember between South Park and Redlands Canyon. Section labels correspond to those in Fig. 4. B) Section-scale: Light blue lines outline the dolomitization front within the Thorndike submember. On the overlain δ^{13}C plot, points correspond to approximate stratigraphic position; blue points are limestone samples and green points are dolostone samples. C) Outcrop-scale: Images of the base of the dolomitized interval. Note the sharp, but irregular contact of the dolomitization, as well as the diffuse zone of dolomite veins proximal to the contact. On the overlain δ^{13}C plot, dark blue points are limestone and light blue points are dolomite. Values correspond to precise sample locations. D) Hand sample-scale: Drilled hand samples demonstrate high variability in δ^{13}C values on a cm-scale across the dolomitization front. δ^{18}O values are plotted in parentheses for comparison.

ganic carbon concentrations in the unlithified sediment and coeval pore fluids of this unit, as organic matter could have been remobilized at a number of later stages including remineralization during early diagenesis, hydrocarbon migration, graphitization during burial metamorphism associated with Mesozoic orogenesis (Labotka et al., 1985), and oxidation by hydrothermal fluids associated with Miocene basin and range extension. Some of the other Cryogenian units in the Panamint Range (Limekiln Spring and Sourdough Limestone members) contain significant graphite enrichments (locally >1%), which have been interpreted as organic carbon in origin (Carlisle et al., 1980; Miller, 1985). Therefore, it is conceivable that this basin was a favorable environment for high productivity and that these mid-Cryogenian sediments, including

those of the Middle Park, initially contained significant concentrations of organic carbon.

5.2. Chemostratigraphy of the Thorndike

The Thorndike submember is a carbonate platform deposit formed within shallow subaqueous environments of a partially restricted basin (see Geological Setting). Limestone of the Thorndike submember preserves highly ^{13}C-enriched δ^{13}C values ($\sim$+4 to +9‰), but dolostone samples within laterally equivalent strata preserve significantly lower δ^{13}C values ($\sim$-4 to +3‰) with δ^{13}C differences of up to 10‰. Since the isotopic alteration tracks mapped dolomitization fronts, which are irregular and occur at multiple stratigraphic levels, this range in δ^{13}C values cannot be explained
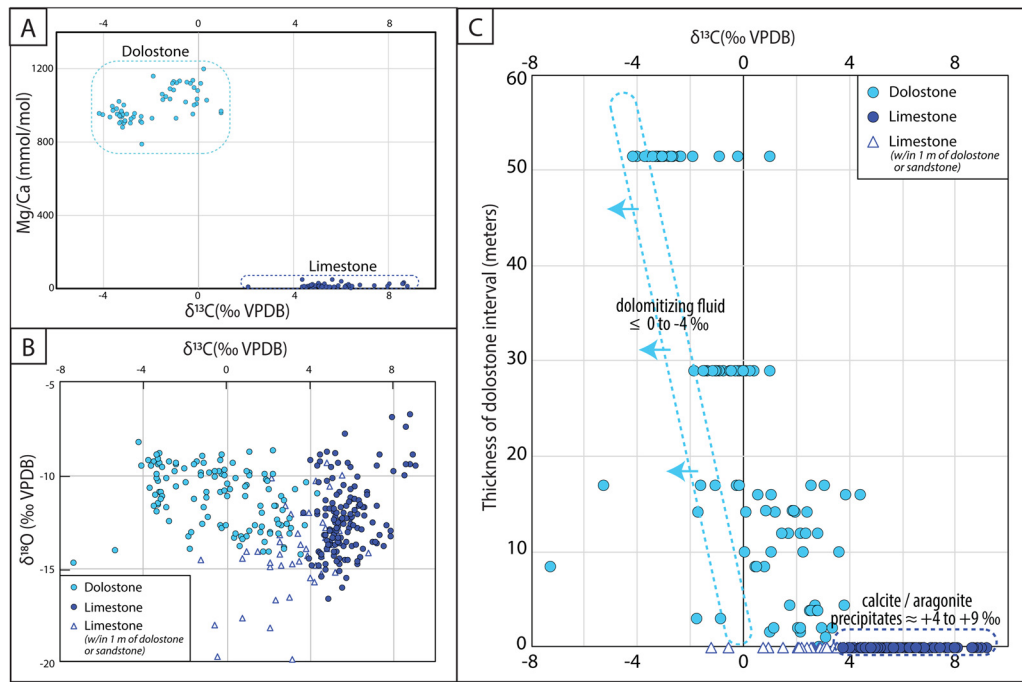
Fig. 6. Cross plots showing mineralogy-dependent variability in δ^{13}C within Thorndike submember. A) Mg/Ca vs. δ^{13}C for sections L1502, L1509, and L1603 of Thorndike submember. B) δ^{18}O vs. δ^{13}C cross plot for samples from all sections of Thorndike submember. C) δ^{13}C values plotted against thickness of dolomitized interval they occur within, demonstrating that thicker zones of dolomitization have lower δ^{13}C values. Dolomite and limestone samples are in different colors. Limestone samples within 1-m of a dolostone or siliciclastic bed are plotted as triangles.

by laterally diachronous deposition of the Thorndike submember or, consequentially, interpreted to reflect variation in primary seawater DIC values (Fig. 4).

The timing of the dolomitization is critical to understanding the mechanism for isotopic alteration. The overlying Marinoan-age Wildrose diamictite contains abundant clasts of both dolostone and limestone that were clearly derived from the underlying Thorndike submember, which requires that dolomitization occurred during or prior to the Marinoan glaciation. Carbon isotope values of clasts within the Wildrose diamictite range from -1 to +9‰, with dolostone clasts statistically lighter than limestone clasts (Fig. 7), comparable to the variability observed in the underlying Thorndike (Fig. 4). Curiously, some dolostone clasts are associated with recrystallized rims of calcite that have δ^{13}C values that are elevated by up to 4‰ compared to the clast interiors (N=6), and have lower and more consistent δ^{18}O values that trend towards ∼-13‰ (Fig. 7F,G). The isotopic differences of these reaction rims are consistent with burial-related de-dolomitization of the clasts, possibly associated with the same stage of diagenesis as sediment-buffered neomorphism of aragonite to calcite within the underlying Thorndike submember. Fluids associated with this neomorphism would have been carbon buffered by ^{13}C-enriched limestone of the underlying Thorndike submember, and the recrystallized carbonates would have had relatively consistent and lower δ^{18}O composition associated with an elevated burial temperature (Fig. 6B). Under this scenario, the isotopic signatures on the de-dolomitized reaction rims of the Wildrose clasts are recording this later stage of burial-related neomorphism, while the dolomitization within the Thorndike submember and associated δ^{13}C alteration occurred prior to the deposition of the Wildrose submember.

Based on existing radiometric age constraints and the mineralogy and δ^{13}C values of carbonate clasts within the Wildrose, dolomitization and δ^{13}C alteration within the Thorndike must have occurred after deposition <652 Ma and before the end of the Marinoan glaciation at 635 Ma (Nelson et al., 2020). Since platform dolomitization is driven by subsurface fluid flow, which is en-

hanced by sea-level fluctuations (Kaufman, 1994), this relatively early dolomitization may have been related to either local, tectonically driven base level change or eustatic change forced by Cryogenian climate. The lateral variability of the dolomitization front may be explained by: 1) disparities in initial porosity of the carbonate; 2) proximity to basin faults active during times of fluid migration; and/or 3) depositional position on the carbonate platform (platform interior, rim, foreslope). Given the high Mg^{2+} budget and fluid flow requirements for post-depositional dolomitization, modification of δ^{13}C values by dolomitizing fluids is conceptually reasonable. Similarly, δ^{13}C variability of up to 5‰ has been documented between limestone and dolostone in Cryogenian and Ediacaran sections from Mongolia (Bold et al., 2016, 2020). The observations from both the Thorndike and units in Mongolia demonstrate the ability of early-burial dolomitization to drastically alter δ^{13}C values. In the case of the Thorndike submember, the dolomitizing fluid must have been significantly ^{13}C-depleted, based on the directionality and extent of the alteration, which may help characterize the diagenetic processes operating within Neoproterozoic carbonate platforms.

Calcium and magnesium isotopes of carbonate rocks have been established as useful tracers of marine diagenesis and can be used to discriminate between seawater- and sediment-buffered diagenesis (Ahm et al., 2018; Higgins et al., 2018). Modern to recent dolomite that formed during early-marine diagenesis in a fluid-buffered setting tend to have high $\delta^{44/40}$Ca values that approach modern seawater (0‰) and low δ^{26}Mg values that are 2‰ lighter than modern seawater (∼-2.8‰, Higgins and Schrag, 2010). This offset of δ^{26}Mg values from seawater has been suggested to be the result of a Mg isotope fractionation factor of ∼0.9980 associated with the recrystallization of low-Mg calcite and dolomite (Higgins and Schrag, 2010; Fantle and Higgins, 2014; Higgins et al., 2018), while the $\delta^{44/40}$Ca values are similar to seawater because the Ca isotope fractionation factor associated with recrystallization approaches ∼1.0000 (Fantle and DePaolo, 2007). In contrast, dolomites formed under sediment-buffered conditions have
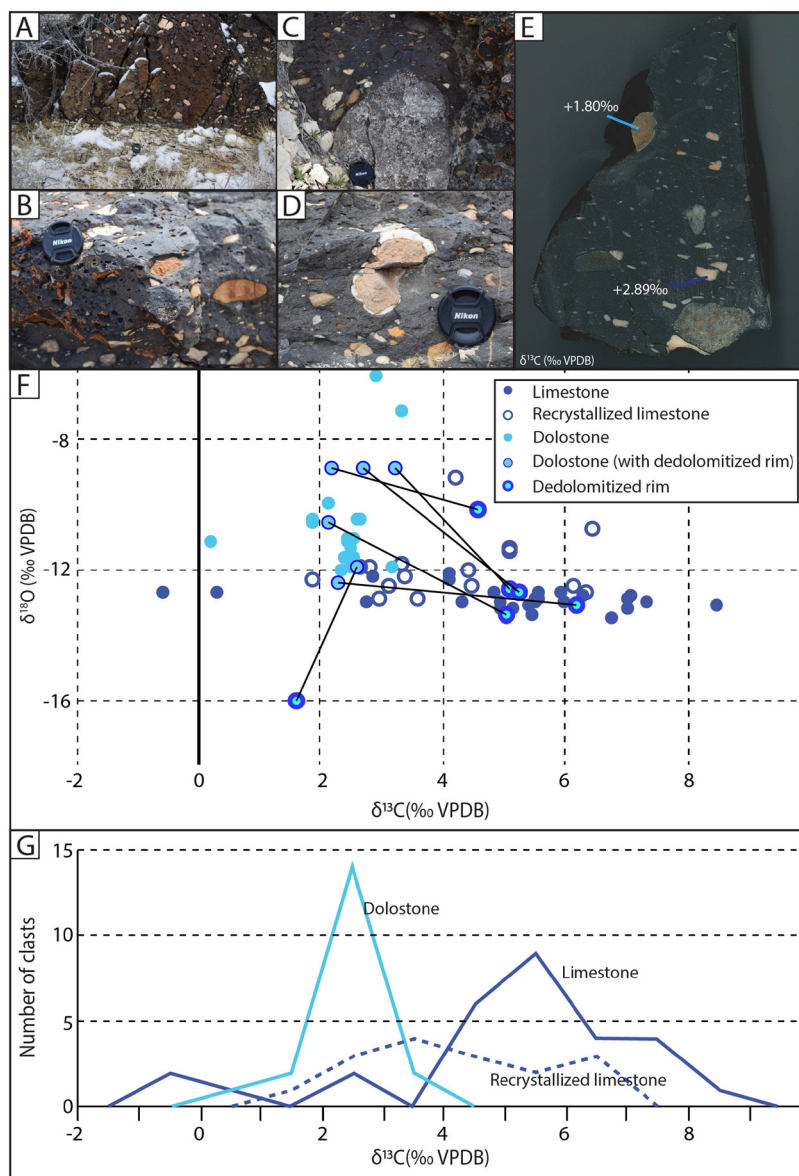
Fig. 7. Field photographs and $\delta^{13}C$ data of the Wildrose submember. A) Wildrose diamictite erosively overlies the Thorndike submember, and basal portion is dominated by carbonate clasts of the Thorndike submember. B, C, E) There are both limestone and dolostone clasts within the basal Wildrose indicating dolomitization predated erosion of the Thorndike and deposition of the Wildrose—dolomite clasts are tan; limestone clasts are blue with lamination textures or white and recrystallized. D) Dolomite clast with dedolomitized rim. F) $\delta^{13}C$ values of various types of carbonate clasts within diamictite of the Wildrose submember sampled between South Park and Redlands Canyon suggest that dolomitization altered the carbon isotope values of the Thorndike prior to deposition of the Wildrose. Some dolostone clasts have dedolomitized reaction rims (pairs of rim and clast center are connected via lines), which show significant $\delta^{13}C$ alteration. G) Binned frequency of $\delta^{13}C$ clast composition by mineralogy. Coarsely recrystallized calcite clasts are distinguished from laminated limestone clasts that preserve sedimentary textures.

$\delta^{44/40}Ca$ values within the range of the precursor carbonate sediments ($\sim$-1.5 to -1.0‰, Gussone et al., 2005) and $\delta^{26}Mg$ values that are variably enriched from -2.8‰ (due to Raleigh-type distillation, Fantle and Higgins, 2014; Blättler et al., 2015).

Calcium isotope values of the Thorndike limestone are within the range of modern calcite precipitates and bulk silicate Earth that, on average, are -1‰ depleted in $\delta^{44/40}Ca$ relative to modern seawater (Fig. 8; Blättler and Higgins, 2017; Gussone et al., 2020). The $\delta^{44/40}Ca$ values of the Thorndike dolomite samples are within the same range as the limestone samples, and the $\delta^{26}Mg$ values are ^{26}Mg-enriched (Fig. 8). These values indicate that the dolomitizing fluids were significantly evolved from coeval seawater (sediment-buffered dolomitization), since reactions with the surrounding sediment caused $\delta^{44/40}Ca$ values to become lower and $\delta^{26}Mg$ values to become higher.

Previously, high $\delta^{13}C$ values of the Thorndike have been attributed to global processes that led to ^{13}C-enriched marine DIC, and thus correlated to highly positive values recorded in other Cryogenian carbonate strata globally termed the "Keele peak" (e.g., Halverson et al., 2005). Based on the regional stratigraphic and sedimentological evidence for partial restriction of the Thorndike carbonate platform, as well as the geochemical data presented herein, we suggest an alternative local explanation for these high $\delta^{13}C$ values that does not require extreme global seawater DIC composition. Below, we explore possible mechanisms for producing ^{13}C-enriched and ^{13}C-depleted $\delta^{13}C$ values within the limestone and dolostone, respectively, of the Thorndike submember.

High $\delta^{13}C$ values of Thorndike limestone may reflect intense local primary productivity on the platform top, which led to ^{13}C-enriched DIC in surface waters, as has been proposed to explain ^{13}C-enriched DIC on the Bahama Banks relative to modern ma-
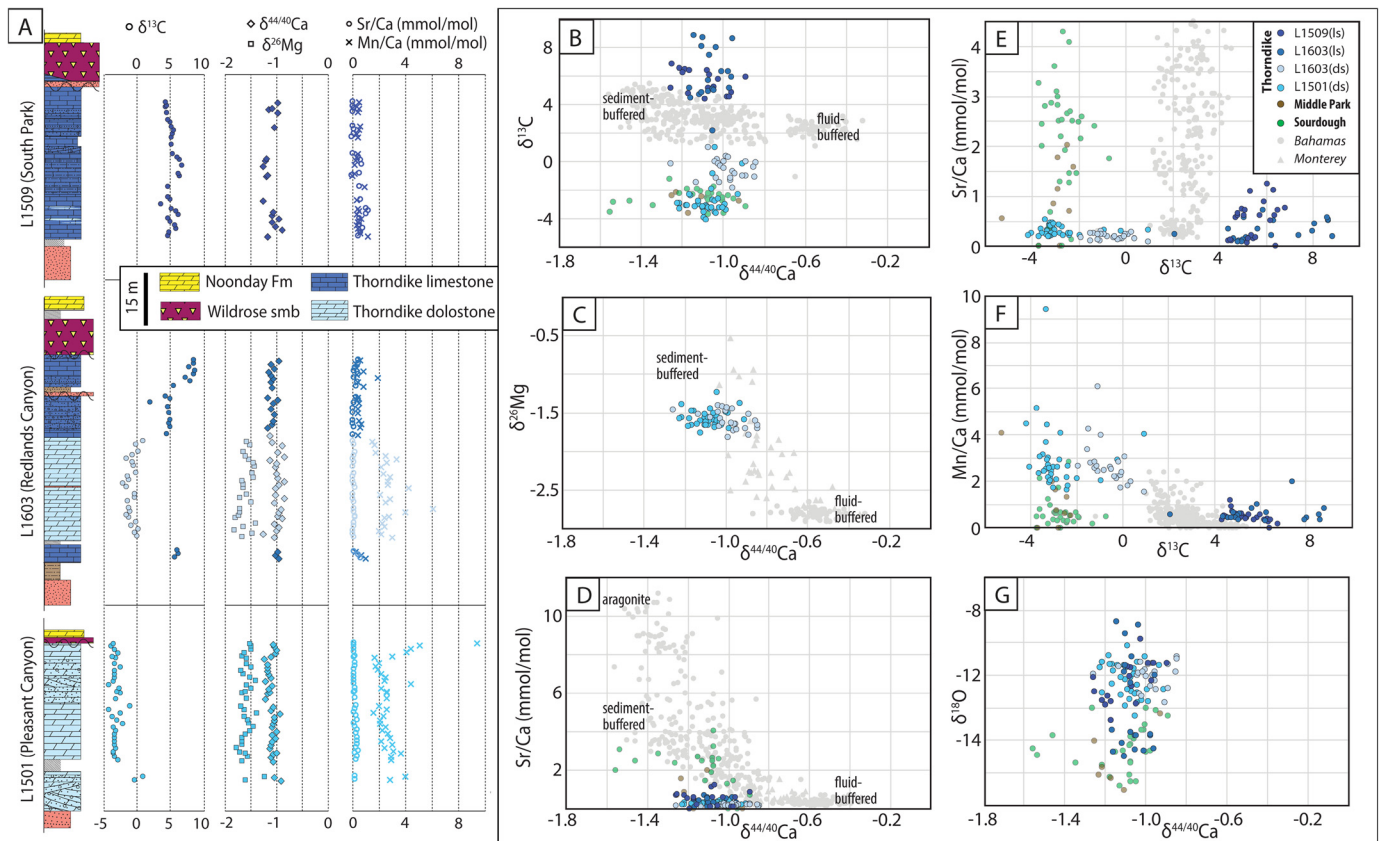
Fig. 8. A) Lithostratigraphy of Thorndike submember sections L1502, L1509, and L1603 with $\delta^{13}C$, $\delta^{44/40}Ca$, $\delta^{26}Mg$, Sr/Ca, and Mn/Ca data. Note dolostone and limestone samples are different colors and correspond to colors in cross plots. B-G) Cross plots comparing $\delta^{13}C$, $\delta^{18}O$, $\delta^{44/40}Ca$, $\delta^{26}Mg$, Sr/Ca, and Mn/Ca data from Sourdough Limestone Member, Middle Park submember, and Thorndike submember. Geochemical data from Miocene–Holocene carbonates from the Bahamas and authigenic dolomite from the Neogene Monterey Formation plotted for comparison (Blättler et al., 2015; Ahm et al., 2018; Higgins et al., 2018). ls—limestone; ds—dolostone.

rine DIC (Swart et al., 2009; Geyman and Maloof, 2019). Alternatively, rather than being produced within platform top waters, ^{13}C-enriched DIC could have been produced within pore fluids by high local oxygenic phototrophic productivity within oxic pore spaces of stromatolite reefs, microbial mats, or grainstones, adjacent to the sediment-water interface (Fig. 9A). Even though much of the Thorndike carbonate sediment is traction-bedded grainstone, the original precipitation of these carbonate minerals prior to transport may have occurred primarily within microbially influenced pore spaces. Another potential source of ^{13}C-enriched authigenic carbonate is within the methanogenesis zone, particularly if ^{13}C-depleted methane escapes as gas before remineralization (Hayes and Waldbauer, 2006; Birgel et al., 2015). While methanogenesis can decrease the carbonate saturation of pore waters, leading to carbonate dissolution rather than precipitation, carbonate can form where CO_2 production is offset by alkalinity production from phototrophic CO_2 fixation or anaerobic methane oxidation (Fig. 9A; Moore et al., 2004; Birgel et al., 2015). Although this type of balanced metabolic competition may be an implausible mechanism for production of the large volumes of authigenic carbonate necessary to lead to stratigraphically and laterally consistent $\delta^{13}C$ values at scale — such as those observed within limestone of the Thorndike submember for >80 m of strata across >50 km (Fig. 4) — it is possible this scale of carbonate precipitation could be supported during the Proterozoic by increased background carbonate supersaturation in ocean and/or pore fluids (Grotzinger and James, 2000; Higgins et al., 2009; Birgel et al., 2015).

The relatively low $\delta^{13}C$ values recorded in dolostone of the Thorndike submember (Figs. 4–6) indicate the DIC of dolomitizing fluids had a significantly lower $\delta^{13}C$ composition than the fluids

from which the limestone precipitated. If dolomitization resulted from reflux circulation of platform waters, then ^{13}C-depleted fluids could have resulted from kinetic isotope effects related to CO_2 invasion in surface waters (e.g., Ahm et al., 2019), as conjectured above for the Sourdough Limestone Member and Middle Park submember. Alternatively, the low $\delta^{13}C$ composition could be the product of organic carbon remineralization along the flow path of the dolomitizing fluid within platform waters and/or pore fluids, which is consistent with the sediment-buffered $\delta^{44/40}Ca$ and $\delta^{26}Mg$ values accompanying negatively altered $\delta^{13}C$ values. In this model, as fluids migrated across this partially restricted platform top and flushed through it, either through brine reflux or thermal convection (Fig. 9B; e.g., Kaufman, 1994), they became sediment-buffered with respect to Ca^{2+} and Mg^{2+} and diverged from the $\delta^{13}C$ composition of seawater DIC. However, rather than simply inheriting $\delta^{13}C$ values from the precursor carbonate sediments (which were ^{13}C-enriched), these dolomitizing fluids also incorporated remineralized organic carbon through aerobic respiration on the platform top and/or from zones of anaerobic organic carbon remineralization within the precursor sediment pore fluids, leading to ^{13}C-depleted DIC within the fluids relative to the sediment (Fig. 9; Malone et al., 2002; Meister and Reyes, 2019). We suggest that these fluids dolomitized portions of the platform, forming early-burial diagenetic dolomite with relatively ^{13}C-depleted $\delta^{13}C$ values. An organic carbon remineralization mechanism for the production of ^{13}C-depleted dolomite is supported by the high Mn/Ca ratios of the Thorndike dolostone relative to the precursor limestone (Fig. 8F; even accounting for differences in Mg/Ca), which suggest the dolomitizing fluids were reducing. This interpretation is further supported by a correlation between dolomite bed thick-
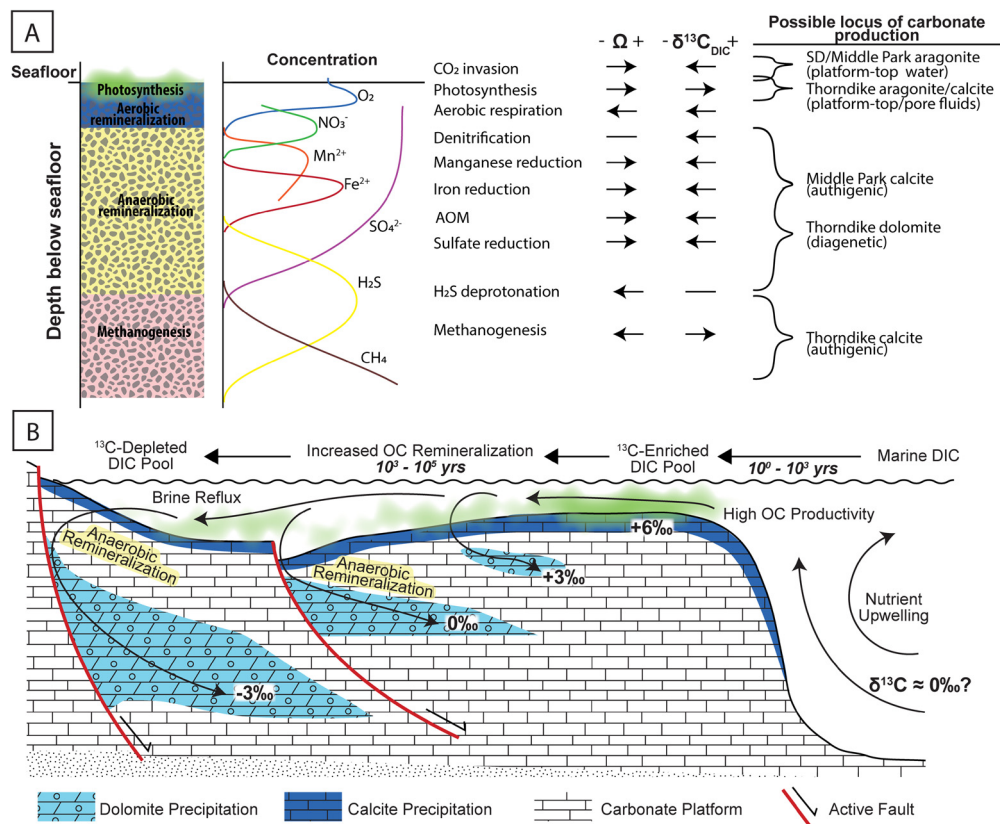
Fig. 9. A) Schematic subsurface redox profile beneath oxygenated bottom waters (Jørgensen and Kasten, 2006). The effects on pore water carbonate saturation (Ω) and DIC $\delta^{13}C$ composition of various subsurface organic carbon production and remineralization pathways (Ohmoto, 1972; Malone et al., 2002; Higgins et al., 2009; Bergmann et al., 2013; Meister and Reyes, 2019). Probable loci of authigenic carbonate production to produce observed $\delta^{13}C$ values of the Thorndike and Middle Park submembers. B) Schematic model for isotopic alteration by platformal dolomitization within the Thorndike submember. Thicker intervals of dolostone form from longer fluid pathways, with more opportunity to incorporate ^{13}C-depleted remineralized organic carbon, resulting in a relationship between dolomite thickness and $\delta^{13}C$ values. DIC—dissolved inorganic carbon; OC—organic carbon; AOM—anaerobic oxidation of methane.

ness and depletion of $\delta^{13}C$ (Fig. 6C). Within a reflux dolomitization scenario, dolomitizing fluids with a longer flow path had more opportunity to incorporate ^{13}C-depleted DIC through organic carbon remineralization (Fig. 9), and, moreover, larger volumes of fluid had higher oxidant loads and were less sediment-buffered by the ^{13}C-enriched precursor limestone.

Based on the integrated data from this unit, we interpret the Thorndike submember $\delta^{13}C$ values as records of platform organic carbon production and remineralization, which led to extreme $\delta^{13}C$ values of local pore water DIC (Fig. 9). In this model, neither the original calcite nor subsequent dolomite precipitates of the Thorndike submember record $\delta^{13}C$ values that are representative of global Cryogenian seawater. Therefore, the widely correlated Keele peak could be a product of local organic carbon productivity and/or kinetic isotopic effects associated with carbonate precipitation and degassing on microbially dominated carbonate platforms (Hoffman and Lamothe, 2019; Geyman and Maloof, 2019; Beeler et al., 2020), rather than the record of an extreme global DIC composition that would require exceptionally high organic carbon export. The ability of seawater-buffered diagenesis to alter $\delta^{13}C$ values within carbonate platforms has been demonstrated as a major lever on both modern and ancient carbon isotope records (Ahm et al., 2018, 2019; Higgins et al., 2018; Hoffman and Lamothe, 2019). Importantly, the dataset from the Panamint Range suggests that sediment-buffered diagenesis also has the ability to significantly alter $\delta^{13}C$ values, and we suggest this occurs through variations in the production and remineralization of organic carbon within the pore waters of partially restricted platform settings.

5.3. Neoproterozoic carbon isotope record and microbial carbonates

We speculate that localized organic carbon production and remineralization could have been an important lever on $\delta^{13}C$ values of carbonates during the microbially dominated Neoproterozoic. Since the $\delta^{13}C$ record is predominantly from carbonate rocks, it is fundamentally tied to carbonate sediment production, which is recognized to have varied significantly through Earth history (e.g., Grotzinger and James, 2000). Following the establishment of the skeletal carbonate factory in the late Cambrian, global carbonate production during the Phanerozoic was dominated by skeletal carbonate minerals produced by biomineralizing organisms (both metazoans and algae) within the water column and therefore in relative equilibrium with the DIC of seawater (assuming only minor kinetic effects). However, in the Proterozoic and Cambrian, carbonate production was likely restricted to shallow-water platforms dominated by microbial mats. In these settings, carbonate minerals were primarily produced within microbially influenced environments, such as beneath biofilms in inter-mat spaces or pore waters, and precipitated from fluids that were restricted from seawater and thus from the global DIC pool (Visscher and Stolz, 2005). If the bottom waters of these platform environments were oxygenated, the subsurface pore waters could have large redox gradients spanning fully aerobic to anaerobic and methanogenic redox zones (Fig. 9A).

The redox zones of pore waters would control (1) the carbonate saturation state of the pore waters (Visscher and Stolz, 2005; Higgins et al., 2009; Bergmann et al., 2013), (2) the rates of organic carbon production and remineralization, and (3) the $\delta^{13}C$ composi-
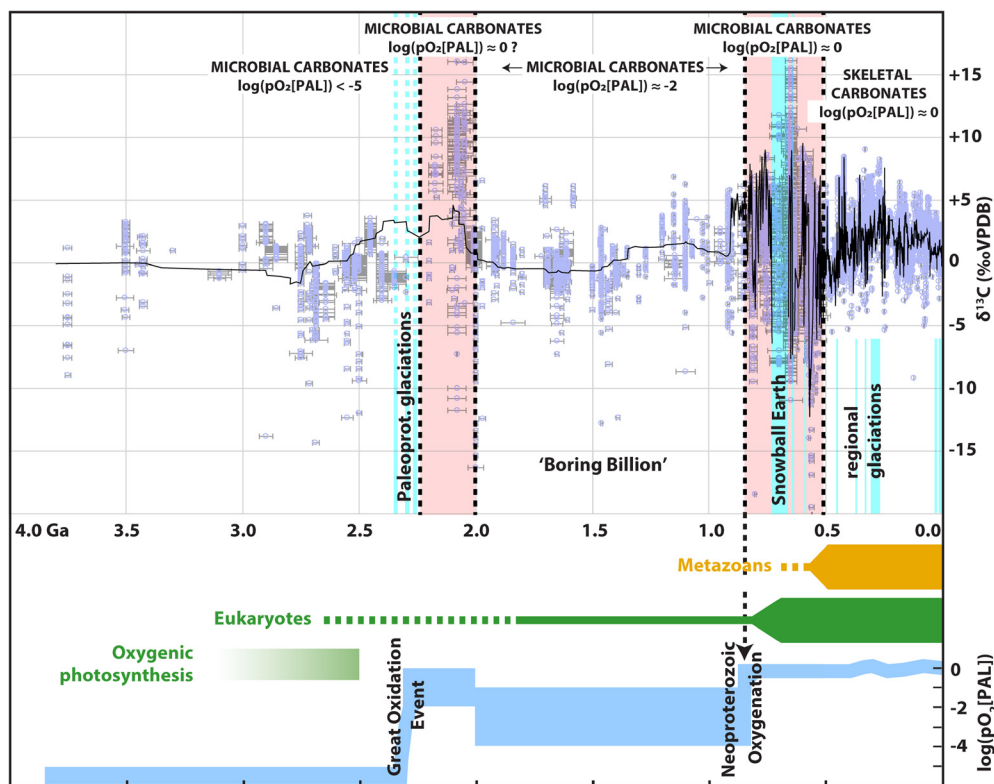
Fig. 10. The carbon isotope record of Earth's carbonates. $\delta^{13}C_{carb}$ data points from Prokoph et al. (2008). Composite $\delta^{13}C$ curves from Shields and Veizer (2002) (Archean–Mesoproterozoic), modified from Halverson et al. (2005) (Neoproterozoic), and from Saltzman and Thomas (2012) (Cambrian–Quaternary). Pink shading indicates intervals of high $\delta^{13}C$ variability that is attributed to elevated subsurface pore water redox gradients. PAL—present atmospheric level.

tion of pore water DIC (Ohmoto, 1972; Malone et al., 2002; Meister and Reyes, 2019). Therefore, the $\delta^{13}C$ composition of authigenic carbonate precipitated below the sediment-water interface – the dominant space of carbonate precipitation in the Proterozoic microbial world – resulted from the relative locus of mineralization within the framework of this diagenetic redox profile (Fig. 9A). Moreover, both the locus of mineralization and structure of the redox profile would be controlled by local factors such as the amount of organic carbon within the unlithified sediments, sediment porosity, relative openness of the system to fluid flow, and sedimentation rates. Large swings in the $\delta^{13}C$ record of platform carbonates formed under these microbially influenced conditions are consistent with local variations in sedimentary facies, rather than global changes to the surface carbon cycle.

For example, in carbonate platforms dominated by stromatolite reefs and grainstones with high porosities (relatively open-system), primary productivity could leave behind a ^{13}C-enriched pool of DIC from which to precipitate authigenic carbonate with positive $\delta^{13}C$ values, such as those seen in limestone of the Thorndike submember, which could be preserved if open-system behavior allowed organic carbon remineralization to be temporally or spatially separated from this precipitation. Conversely, in a depositional system of interbedded mudstone and carbonate (more closed-system settings), these siliciclastic layers could form seals on fluid migration after burial and compaction, preventing this open-system behavior during diagenesis. Anaerobic remineralization of organic carbon during diagenesis within such a closed system could produce a ^{13}C-depleted pool of DIC within the pore waters from which to precipitate authigenic carbonate with negative $\delta^{13}C$ values, such as those seen in limestone of the Middle Park submember. Depending on the specific conditions and fluid pathways, diagenetic dolomitization could introduce either marine DIC or fluids that are significantly evolved from marine DIC with altered isotopic compositions (such as those that dolomitized the Thorndike submember).

If local sediment burial conditions and carbonate facies were the primary controls on $\delta^{13}C$ values, broadly correlative carbon isotope excursions, such as the Rasthof, Keele, and Trezona anomalies during the Cryogenian, can potentially be explained by regionally or globally consistent sedimentation and dolomitization patterns, controlled by factors such as margin-wide or global changes in sea level, climate, or tectonism.

If local carbonate platform processes contributed to the widespread, extreme variability in $\delta^{13}C$ values observed during the Neoproterozoic and early Cambrian, why is such variability not observed in microbially dominated carbonate platforms of the Mesoproterozoic (Fig. 10)? An implication of the outlined model is that a significant subsurface redox gradient was necessary to drive variation in carbon speciation, and thus $\delta^{13}C$ variability, within microbially mediated authigenic carbonates (Fig. 9). This suggests that the onset of large magnitude carbon isotope excursions in the Tonian (i.e. Bitter Spring anomaly) resulted from an increase in the oxygen levels of marine environments at this time (Fig. 10; Hoffman and Lamothe, 2019), which has been increasingly supported by other lines of evidence (e.g., Cole et al., 2016; Planavsky et al., 2018). Furthermore, this model may explain large $\delta^{13}C$ variability associated with the Great Oxidation Event and the subsequent Lomagundi excursion (e.g., Mayika et al., 2020). It has been suggested that after the Lomagundi excursion at ~2.05 Ga, oxygen levels decreased again (Bekker and Holland, 2012), perhaps associated with lower global primary productivity (Hodgskiss et al., 2019). Empirical evidence and models are consistent with the continuation of low oxygen (<1% present atmospheric level) and low marine primary productivity (<3% present level) throughout the mid-Proterozoic from ~2.05-0.81 Ga (e.g., Crockford et al., 2018; Planavsky et al., 2018). We suggest these environments lacked the requisite levels of surface productivity and subsurface redox gradients, even within microbially dominated carbonate platforms, to

drive localized large carbon isotope variability within platform and pore waters.

6. Conclusions

We present δ^{13}C, $\delta^{44/40}$Ca, and δ^{26}Mg geochemical data from carbonate strata deposited during the Cryogenian non-glacial interlude in the Panamint Range, California. Negative δ^{13}C values preserved for >100 m in the post-Sturtian Sourdough Limestone Member and Middle Park submember suggest an expanded record of the aftermath of the Sturtian glaciation. These are accompanied by relatively low $\delta^{44/40}$Ca values and high Sr/Ca ratios, consistent with primary aragonite sedimentation for Sturtian cap carbonates, which were sediment buffered in this environment due to high sedimentation rates. Persistent negative δ^{13}C values may have been produced through local anaerobic organic carbon remineralization and/or kinetic effects related to CO_2 invasion, both consistent with high platform primary productivity. Within the pre-Marinoan Thorndike submember, early-burial dolomitization drastically shifted δ^{13}C of carbonates, depleting values by up to 10‰ in comparison to stratigraphically equivalent limestone. Geochemical tracers of diagenesis ($\delta^{44/40}$Ca and δ^{26}Mg values) suggest δ^{13}C variability in the Thorndike reflects the evolution of local dissolved inorganic carbon pools within a partially restricted carbonate platform: 1) Highly ^{13}C-enriched δ^{13}C values within limestone samples of the Thorndike resulted from local primary productivity on platform tops or within oxygenated pore waters; and 2) relatively ^{13}C-depleted δ^{13}C values within dolostone resulted from evolved dolomitizing fluids incorporating remineralized organic carbon from platform waters and/or sediment pore space. These results indicate sediment-buffered diagenesis, with respect to Ca and Mg isotopes, can lead to δ^{13}C alteration within carbonates through remineralization of platform top and sediment-hosted organic carbon within pore fluids. Therefore, in some cases, δ^{13}C variability in the Neoproterozoic could reflect variations in local organic carbon production and remineralization within platform top and pore waters, rather than perturbations to the global surface carbon cycle.

CRediT authorship contribution statement

Lyle L. Nelson: Conceptualization, Investigation, Visualization, Writing – original draft. **Anne-Sofie C. Ahm:** Investigation, Writing – review & editing. **Francis A. Macdonald:** Conceptualization, Writing – review & editing. **John A. Higgins:** Resources, Writing – review & editing. **Emily F. Smith:** Conceptualization, Investigation, Supervision, Writing – review & editing.

Declaration of competing interest

The authors declare that they have no known competing financial interests or personal relationships that could have appeared to influence the work reported in this paper.

Acknowledgements

Appendix A. Supplementary material

Supplementary material related to this article can be found online at https://doi.org/10.1016/j.epsl.2021.116956.

References

Ahm, A.S.C., Bjerrum, C.J., Blättler, C.L., Swart, P.K., Higgins, J.A., 2018. Quantifying early marine diagenesis in shallow-water carbonate sediments. Geochim. Cosmochim. Acta 236, 140–159.

Ahm, A.S.C., Maloof, A.C., Macdonald, F.A., Hoffman, P.F., Bjerrum, C.J., Bold, U., Rose, C.V., Strauss, J.V., Higgins, J.A., 2019. An early diagenetic deglacial origin for basal Ediacaran "cap dolostones". Earth Planet. Sci. Lett. 506, 292–307.

Banner, J.L., Hanson, G.N., 1990. Calculation of simultaneous isotopic and trace element variations during water-rock interaction with applications to carbonate diagenesis. Geochim. Cosmochim. Acta 54 (11), 3123–3137.

Beeler, S.R., Gomez, F.J., Bradley, A.S., 2020. Controls of extreme isotopic enrichment in modern microbialites and associated abiogenic carbonates. Geochim. Cosmochim. Acta 269, 136–149.

Bekker, A., Holland, H.D., 2012. Oxygen overshoot and recovery during the early Paleoproterozoic. Earth Planet. Sci. Lett. 317, 295–304.

Bergmann, K.D., Grotzinger, J.P., Fischer, W.W., 2013. Biological influences on seafloor carbonate precipitation. Palaios 28 (2), 99–115.

Birgel, D., Meister, P., Lundberg, R., Horath, T.D., Bontognali, T.R., Bahniuk, A.M., de Rezende, C.E., Vásconcelos, C., McKenzie, J.A., 2015. Methanogenesis produces strong 13C enrichment in stromatolites of Lagoa Salgada, Brazil: a modern analogue for Palaeo-/Neoproterozoic stromatolites? Geobiology 13 (3), 245–266.

Blättler, C.L., Higgins, J.A., 2017. Testing Urey's carbonate–silicate cycle using the calcium isotopic composition of sedimentary carbonates. Earth Planet. Sci. Lett. 479, 241–251.

Blättler, C.L., Miller, N.R., Higgins, J.A., 2015. Mg and Ca isotope signatures of authigenic dolomite in siliceous deep-sea sediments. Earth Planet. Sci. Lett. 419, 32–42.

Bold, U., Smith, E.F., Rooney, A.D., Bowring, S.A., Buchwaldt, R., Dudás, F.Ö., Ramezani, J., Crowley, J.L., Schrag, D.P., Macdonald, F.A., 2016. Neoproterozoic stratigraphy of the Zavkhan terrane of Mongolia: The backbone for Cryogenian and early Ediacaran chemostratigraphic records. Am. J. Sci. 316 (1), 1–63.

Bold, U., Ahm, A.S.C., Schrag, D.P., Higgins, J.A., Jamsran, E., Macdonald, F.A., 2020. Effect of dolomitization on isotopic records from Neoproterozoic carbonates in southwestern Mongolia. Precambrian Res. 350, 105902.

Carlisle, D., Kettler, R.M., Swanson, S.C., 1980. Geological Study of uranium potential of the Kingston Peak Formation, Death Valley Region, California. U.S. Department of Energy Open File Report, Grand Junction 109 p.

Clark, I.D., Fontes, J.C., Fritz, P., 1992. Stable isotope disequilibria in travertine from high pH waters: laboratory investigations and field observations from Oman. Geochim. Cosmochim. Acta 56 (5), 2041–2050.

Cole, D.B., Reinhard, C.T., Wang, X., Gueguen, B., Halverson, G.P., Gibson, T., Hodgskiss, M.S., McKenzie, N.R., Lyons, T.W., Planavsky, N.J., 2016. A shale-hosted Cr isotope record of low atmospheric oxygen during the Proterozoic. Geology 44 (7), 555–558.

Corsetti, F.A., Kaufman, A.J., 2003. Stratigraphic investigations of carbon isotope anomalies and Neoproterozoic ice ages in Death Valley, California. Geol. Soc. Am. Bull. 115 (8), 916–932.

Crockford, P.W., Hayles, J.A., Bao, H., Planavsky, N.J., Bekker, A., Fralick, P.W., Halverson, G.P., Bui, T.H., Peng, Y., Wing, B.A., 2018. Triple oxygen isotope evidence for limited mid-Proterozoic primary productivity. Nature 559 (7715), 613–616.

Derry, L.A., 2010. A burial diagenesis origin for the Ediacaran Shuram–Wonoka carbon isotope anomaly. Earth Planet. Sci. Lett. 294 (1–2), 152–162.

Fantle, M.S., DePaolo, D.J., 2007. Ca isotopes in carbonate sediment and pore fluid from ODP site 807A: the Ca2+ (aq)–calcite equilibrium fractionation factor and calcite recrystallization rates in Pleistocene sediments. Geochim. Cosmochim. Acta 71 (10), 2524–2546.

Fantle, M.S., Higgins, J., 2014. The effects of diagenesis and dolomitization on Ca and Mg isotopes in marine platform carbonates: implications for the geochemical cycles of Ca and Mg. Geochim. Cosmochim. Acta 142, 458–481.

Geyman, E.C., Maloof, A.C., 2019. A diurnal carbon engine explains 13C-enriched carbonates without increasing the global production of oxygen. Proc. Natl. Acad. Sci. 116 (49), 24433–24439.

Grotzinger, J.P., James, N.P., 2000. Precambrian carbonates: evolution of understanding. In: Grotzinger, J.P., James, N.P. (Eds.), Carbonate Sedimentation and Diagenesis in the Evolving Precambrian World, vol. 67. SEPM, pp. 3–20. Special Publication.

Gussone, N., Böhm, F., Eisenhauer, A., Dietzel, M., Heuser, A., Teichert, B.M., Reitner, J., Wörheide, G., Dullo, W.C., 2005. Calcium isotope fractionation in calcite and aragonite. Geochim. Cosmochim. Acta 69 (18), 4485–4494.

Gussone, N., Ahm, A.S.C., Lau, K.V., Bradbury, H.J., 2020. Calcium isotopes in deep time: potential and limitations. Chem. Geol., 119601.

Hayes, J.M., Waldbauer, J.R., 2006. The carbon cycle and associated redox processes through time. Philos. Trans. R. Soc. Lond. B, Biol. Sci. 361 (1470), 931–950.

Halverson, G.P., Hoffman, P.F., Schrag, D.P., Maloof, A.C., Rice, A.H.N., 2005. Toward a Neoproterozoic composite carbon-isotope record. GSA Bull. 117 (9–10), 1181–1207.

Higgins, J.A., Schrag, D.P., 2003. Aftermath of a snowball Earth. Geochem. Geophys. Geosyst. 4 (3), 1028.

Higgins, J.A., Schrag, D.P., 2010. Constraining magnesium cycling in marine sediments using magnesium isotopes. Geochim. Cosmochim. Acta 74 (17), 5039–5053.

Higgins, J.A., Fischer, W.W., Schrag, D.P., 2009. Oxygenation of the ocean and sediments: consequences for the seafloor carbonate factory. Earth Planet. Sci. Lett. 284 (1–2), 25–33.

Higgins, J.A., Blättler, C.L., Lundstrom, E.A., Santiago-Ramos, D.P., Akhtar, A.A., Ahm, A.C., Bialik, O., Holmden, C., Bradbury, H., Murray, S.T., Swart, P.K., 2018. Mineralogy, early marine diagenesis, and the chemistry of shallow-water carbonate sediments. Geochim. Cosmochim. Acta 220, 512–534.

Hodgskiss, M.S., Crockford, P.W., Peng, Y., Wing, B.A., Horner, T.J., 2019. A productivity collapse to end Earth's Great Oxidation. Proc. Natl. Acad. Sci. 116 (35), 17207–17212.

Hoffman, P.F., 2011. Strange bedfellows: glacial diamictite and cap carbonate from the Marinoan (635 Ma) glaciation in Namibia. Sedimentology 58 (1), 57–119.

Hoffman, P.F., Lamothe, K.G., 2019. Seawater-buffered diagenesis, destruction of carbon isotope excursions, and the composition of DIC in Neoproterozoic oceans. Proc. Natl. Acad. Sci. 116 (38), 18874–18879.

Hoffman, P.F., Schrag, D.P., 2002. The snowball Earth hypothesis: testing the limits of global change. Terra Nova 14 (3), 129–155.

Johnston, D.T., Macdonald, F.A., Gill, B.C., Hoffman, P.F., Schrag, D.P., 2012. Uncovering the Neoproterozoic carbon cycle. Nature 483 (7389), 320–323.

Jørgensen, B.B., Kasten, S., 2006. Sulfur cycling and methane oxidation. In: Marine Geochemistry. Springer, Berlin, Heidelberg, pp. 271–309.

Kaufman, J., 1994. Numerical models of fluid flow in carbonate platforms; implications for dolomitization. J. Sediment. Res. 64 (1a), 128–139.

Kennedy, M.J., Christie-Blick, N., Sohl, L.E., 2001. Are Proterozoic cap carbonates and isotopic excursions a record of gas hydrate destabilization following Earth's coldest intervals? Geology 29 (5), 443–446.

Knauth, L.P., Kennedy, M.J., 2009. The late Precambrian greening of the Earth. Nature 460 (7256), 728–732.

Knoll, A.H., Hayes, J.M., Kaufman, A.J., Swett, K., Lambert, I.B., 1986. Secular variation in carbon isotope ratios from Upper Proterozoic successions of Svalbard and East Greenland. Nature 321 (6073), 832–838.

Labotka, T.C., Warasila, R.L., Spangler, R.R., 1985. Polymetamorphism in the Panamint Mountains, California: a 39AR-40AR study. J. Geophys. Res., Solid Earth 90 (B12), 10359–10371.

Lazar, B., Erez, J., 1992. Carbon geochemistry of marine-derived brines: I. 13C depletions due to intense photosynthesis. Geochim. Cosmochim. Acta 56 (1), 335–345.

Malone, M.J., Claypool, G., Martin, J.B., Dickens, G.R., 2002. Variable methane fluxes in shallow marine systems over geologic time: the composition and origin of pore waters and authigenic carbonates on the New Jersey shelf. Mar. Geol. 189 (3–4), 175–196.

Mayika, K.B., Moussavou, M., Prave, A.R., Lepland, A., Mbina, M., Kirsimäe, K., 2020. The Paleoproterozoic Francevillian succession of Gabon and the Lomagundi-Jatuli event. Geology 48 (11), 1099–1104.

Meister, P., Reyes, C., 2019. The carbon-isotope record of the sub-seafloor biosphere. Geosciences 9 (12), 507.

Miller, J.M., 1985. Glacial and syntectonic sedimentation: the upper Proterozoic Kingston Peak Formation, southern Panamint Range, eastern California. Geol. Soc. Am. Bull. 96 (12), 1537–1553.

Moore, T.S., Murray, R.W., Kurtz, A.C., Schrag, D.P., 2004. Anaerobic methane oxidation and the formation of dolomite. Earth Planet. Sci. Lett. 229 (1–2), 141–154.

Nelson, L.L., Smith, E.F., Hodgin, E.B., Crowley, J.L., Schmitz, M.D., Macdonald, F.A., 2020. Geochronological constraints on Neoproterozoic rifting and onset of the Marinoan glaciation from the Kingston Peak Formation in Death Valley, California (USA). Geology 48 (11), 1083–1087.

Oehlert, A.M., Swart, P.K., 2014. Interpreting carbonate and organic carbon isotope covariance in the sedimentary record. Nat. Commun. 5 (1), 1–7.

Ohmoto, H., 1972. Systematics of sulfur and carbon isotopes in hydrothermal ore deposits. Econ. Geol. 67 (5), 551–578.

Petterson, R., Prave, A.R., Wernicke, B.P., Fallick, A.E., 2011. The Neoproterozoic Noonday Formation, Death Valley region, California. Bulletin 123 (7–8), 1317–1336.

Planavsky, N.J., Cole, D.B., Isson, T.T., Reinhard, C.T., Crockford, P.W., Sheldon, N.D., Lyons, T.W., 2018. A case for low atmospheric oxygen levels during Earth's middle history. Emerg. Top. Life Sci. 2 (2), 149–159.

Prave, A.R., 1999. Two diamictites, two cap carbonates, two δ13C excursions, two rifts: the Neoproterozoic Kingston Peak Formation, Death Valley, California. Geology 27 (4), 339–342.

Prokoph, A., Shields, G.A., Veizer, J., 2008. Compilation and time-series analysis of a marine carbonate δ18O, δ13C, 87Sr/86Sr and δ34S database through Earth history. Earth-Sci. Rev. 87 (3–4), 113–133.

Rooney, A.D., Yang, C., Condon, D.J., Zhu, M., Macdonald, F.A., 2020. U-Pb and Re-Os geochronology tracks stratigraphic condensation in the Sturtian snowball Earth aftermath. Geology 48 (6), 625–629.

Rothman, D.H., Hayes, J.M., Summons, R.E., 2003. Dynamics of the Neoproterozoic carbon cycle. Proc. Natl. Acad. Sci. 100 (14), 8124–8129.

Saltzman, M.R., Thomas, E., 2012. Carbon isotope stratigraphy. In: Gradstein, F.M., Ogg, J.G., Schmitz, M.D., Ogg, G. (Eds.), The Geologic Time Scale, pp. 207–232.

Schrag, D.P., Berner, R.A., Hoffman, P.F., Halverson, G.P., 2002. On the initiation of a snowball Earth. Geochem. Geophys. Geosyst. 3 (6), 1–21.

Schrag, D.P., Higgins, J.A., Macdonald, F.A., Johnston, D.T., 2013. Authigenic carbonate and the history of the global carbon cycle. Science 339 (6119), 540–543.

Shields, G., Veizer, J., 2002. Precambrian marine carbonate isotope database: version 1.1. Geochem. Geophys. Geosyst. 3 (6), 1–12. https://doi.org/10.1029/2001GC000266.

Swanson-Hysell, N.L., Rose, C.V., Calmet, C.C., Halverson, G.P., Hurtgen, M.T., Maloof, A.C., 2010. Cryogenian glaciation and the onset of carbon-isotope decoupling. Science 328 (5978), 608–611.

Swart, P.K., 2008. Global synchronous changes in the carbon isotopic composition of carbonate sediments unrelated to changes in the global carbon cycle. Proc. Natl. Acad. Sci. 105 (37), 13741–13745.

Swart, P.K., Reijmer, J.J., Otto, R., 2009. A reevaluation of facies on Great Bahama Bank II: variations in the δ13C, δ18O and mineralogy of surface sediments. Spec. Publ. Int. Assoc. Sedimentol. 41, 47–59.

Tziperman, E., Halevy, I., Johnston, D.T., Knoll, A.H., Schrag, D.P., 2011. Biologically induced initiation of Neoproterozoic snowball-Earth events. Proc. Natl. Acad. Sci. 108 (37), 15091–15096.

Visscher, P.T., Stolz, J.F., 2005. Microbial mats as bioreactors: populations, processes, and products. Palaeogeogr. Palaeoclimatol. Palaeoecol. 219, 87–100.